Stress effects on the Raman spectrum of an amorphous material: Theory and experiment on *a*-Si:H

David A. Strubbe,[1,][*] Eric C. Johlin,[1,2,][†] Timothy R. Kirkpatrick,[2] Tonio Buonassisi,[2] and Jeffrey C. Grossman[1,][‡]

[1]*Department of Materials Science and Engineering, Massachusetts Institute of Technology, Cambridge, Massachusetts 02139, USA*

[2]*Department of Mechanical Engineering, Massachusetts Institute of Technology, Cambridge, Massachusetts 02139, USA*

Strain in a material induces shifts in vibrational frequencies. This phenomenon is a probe of the nature of the vibrations and interatomic potentials and can be used to map local stress/strain distributions via Raman microscopy. This method is standard for crystalline silicon devices, but due to the lack of calibration relations, it has not been applied to amorphous materials such as hydrogenated amorphous silicon (*a*-Si:H), a widely studied material for thin-film photovoltaic and electronic devices. We calculated the Raman spectrum of *a*-Si:H *ab initio* under different strains ϵ and found peak shifts $\Delta\omega = (-460 \pm 10 \text{ cm}^{-1})\text{Tr}\,\epsilon$. This proportionality to the trace of the strain is the general form for isotropic amorphous vibrational modes, as we show by symmetry analysis and explicit computation. We also performed Raman measurements under strain and found a consistent coefficient of $-510 \pm 120 \text{ cm}^{-1}$. These results demonstrate that a reliable calibration for the Raman/strain relation can be achieved even for the broad peaks of an amorphous material, with similar accuracy and precision as for crystalline materials.

Hydrogenated amorphous silicon (*a*-Si:H) is a photovoltaic material which has been studied for decades and used commercially [1,2]. Compared to the more commonly used crystalline Si (*c*-Si), *a*-Si:H has advantages in stronger visible absorption, cheaper and faster fabrication, and the potential for flexible thin-film devices [2]. *a*-Si:H can be used alone or in heterojunction cells where it can passivate the surface of *c*-Si active layers [2,3]. It also has applications for solar water splitting [4], thin-film transistors [5], bolometers [6], particle detectors [7], and microelectromechanical systems [8]. However, widespread adoption has been limited by two important disadvantages: Mobilities degrade under illumination via the Staebler-Wronski effect [9], and efficiencies are significantly limited by low hole mobility [10].

Crystallization to *c*-Si is used to create higher-mobility microcrystalline Si (*μc*-Si) [11,12] and could circumvent low hole mobility in *a*-Si:H by adding nanostructured charge-extraction channels [13]. Conversion to denser *c*-Si induces stress, as does deposition [14], thermal expansion, or other processing. Stress is often large in thin films (and may be inhomogeneous [15]) and is a critical parameter in *a*-Si:H as it affects mobilities [5], defects [16], the Staebler-Wronski effect [17], mechanical failure properties [18], and potentially transport via band bending [19].

A standard technique to understand stress effects on *c*-Si microelectronic devices is Raman microscopy [20,21], which yields a spatial distribution of stress in the device (unlike x-ray diffraction measurements [22]). The Raman-active optical phonon modes in *c*-Si are shifted to higher frequency by compressive strain (and *vice versa*), with established coefficients [23,24] which are used to translate peak positions to local strain. Raman microscopy is also commonly used for *a*-Si:H and *μc*-Si, generally for mapping the quality or crystallinity of films via the position and width of the transverse optical (TO) peak [11] (analogous to the optical phonons of *c*-Si). In contrast to the case for *c*-Si, for *a*-Si:H the relation between peak positions and strain has not been clear, preventing detailed understanding of stress; with accurate knowledge of the coefficient, these studies would be able to map stress too. This property also serves as a probe of vibrations and interatomic potentials [24,25]. Stress effects on Raman peaks (also called "piezo-Raman" or "phonon deformation potentials") have been studied for various crystalline semiconductors [26]. However there has been little work on amorphous materials, confined to experimental reports on carbon [27] or carbon and SiC fibers [28], without theory or consideration of dependence on strain pattern.

In previous work, Fabian and Allen [25] calculated the effect of hydrostatic pressure on the vibrational modes of large supercells of *a*-Si (nonhydrogenated) via Stillinger-Weber classical potentials but did not compute Raman spectra. An *ab initio* study [29] calculated vibrational modes (but not stress effects) by density-functional theory but obtained Raman spectra only via semiempirical bond polarizability models, which gave a significant discrepancy from experiment.

Experimental work by Ishidate *et al.* [30] and Hishikawa [31] studied the effect of pressure and bending on the Raman spectrum of *a*-Si:H. However, it is not clear how to extract a strain coefficient (the general materials property) from these works, due to insufficient detail about the experimental setups and stress applied [32]. Therefore only qualitative interpretations of *a*-Si:H stress from Raman spectroscopy have been possible [12,33].

In this Rapid Communication, we present a fully *ab initio* computation of the Raman spectrum of *a*-Si:H under neutral and applied strain, complemented with a systematic experimental study. We show the general form of peak shifts with strain in an amorphous material and obtain close agreement between theory and experiment in the spectra and the strain coefficient for the TO peak shift. This provides the calibration needed for quantitative strain mapping of *a*-Si:H films for optical, electronic, and mechanical devices, with

———————
[*]dstrubbe@mit.edu

[†]Present address: FOM Institute AMOLF, 1098 XG Amsterdam, The Netherlands.

[‡]jcg@mit.edu

sufficient sensitivity for applications of interest (analyzed in the Supplemental Material [34]).

Our theoretical calculations use an ensemble of periodic structures generated by the standard classical Monte Carlo Wooten-Winer-Weaire approach [35], representing local regions which are averaged to find the overall properties of *a*-Si:H. We add hydrogen to the sample by breaking randomly chosen Si-Si bonds at the beginning of the process, as in our previous work [36] and implemented in our CHASSM code [37,38]. We use 34 structures to obtain a smooth Raman spectrum, each with formula $Si_{64}H_6$ to emulate a typical 10% hydrogen content, in a cube roughly 11 Å on a side [34]. Density-functional theory (DFT) and density-functional perturbation theory [39] calculations were performed with the QUANTUM ESPRESSO code (version 5.1) [40] and the local-density approximation [41] to obtain the phonons at $\mathbf{q} = \Gamma$ and their first-order Raman intensities [42]. These widely used calculation methods have been found to be generally reliable for vibrational properties [39]. Each structure was calculated also with 0.5% uniaxial compressive and tensile strain, which gave a resolvable effect within a linear regime. We study the unpolarized (isotropically averaged) Raman spectrum, with a Gaussian broadening of 5 cm^{-1} standard deviation, comparable to the separation between vibrational modes in an individual structure.

We benchmark the accuracy of our theoretical approach for strain effects on the Raman spectrum by calculations on *c*-Si under [100] uniaxial strain. The Raman-active zone-center optical phonons have a frequency of 514 cm^{-1}, a typical DFT level of agreement with the experimental value of 520 cm^{-1}

[43]. The slopes of the split modes are in reasonable agreement with the measured values for bulk *c*-Si [24], though slightly too small: singly-degenerate, calculated -424 cm^{-1} vs measured $p/2\omega_0^c = -481 \pm 20$ cm^{-1}; doubly-degenerate, calculated -547 cm^{-1} vs measured $q/2\omega_0^c = -601 \pm 20$ cm^{-1}.

For the experimental measurements, intrinsic *a*-Si:H films were deposited using a plasma-enhanced chemical vapor deposition tool (PECVD, Surface Technology Systems) to a thickness of $\sim 1.1\,\mu$m, on 3-inch-diameter 100 μm ($\pm 15\,\mu$m) thick $\langle 100 \rangle$ *c*-Si wafers. Raman microscopy was performed using a Horiba LabRam-HR800 Raman spectrometer with a 632.8 nm excitation beam focused to a 1 μm spot size. Compressive stress was applied to the *a*-Si:H film by bending the wafer in a custom-built four-point bending apparatus, as shown in the inset of Fig. 1.

The obtained Raman spectra are shown in Fig. 1. The experimental results have been "reduced" by multiplication by the factor $\omega(1 - e^{-\hbar\omega/kT})$ (where ω is the Raman shift and $T = 300$ K is the temperature), which is the basis for Raman temperature determination [44]. We can then directly compare to the calculated absolute Raman intensities [42,45], in arbitrary units since we do not have an experimental intensity calibration. The peaks in *a*-Si:H are conventionally named by the corresponding peaks in the vibrational density of states of *c*-Si [45,46]. The position of the transverse optical (TO) peak, the focus of this work, is at 470 cm^{-1} (theory) and 480 cm^{-1} (experiment), which agrees well within the typical errors of DFT and the variation among *a*-Si:H samples [31]. An example calculated vibrational mode in the TO peak is shown in the inset of Fig. 1. The longitudinal optical
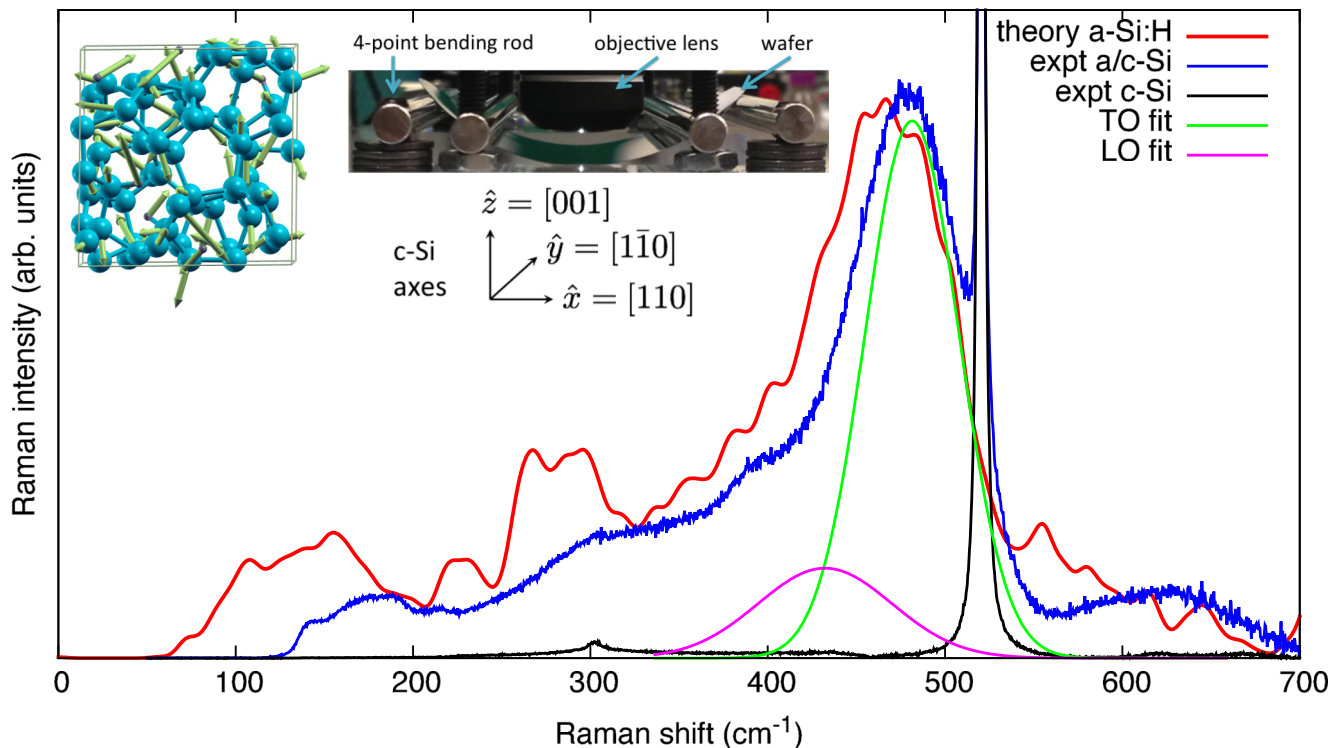

FIG. 1. (Color online) Theoretically calculated Raman spectrum for *a*-Si:H, and measured Raman spectra for *a*-Si:H on *c*-Si, and *c*-Si, reduced by removal of the temperature- and frequency-dependent factors (see text), with fits to *a*-Si:H transverse and longitudinal optical peaks (TO, LO) in measured spectrum. Left inset: Example calculated $Si_{64}H_6$ TO vibrational mode. Right inset: Experimental setup for Raman microscopy with four-point bending and orientation of crystal axes in *c*-Si wafer.
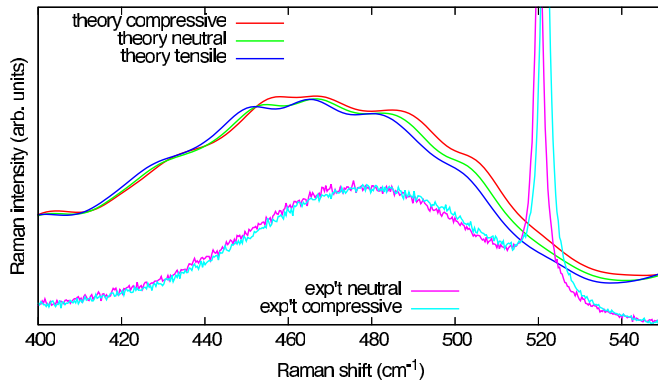
FIG. 2. (Color online) Effect of strain on the Raman spectra: theoretical calculations of a-Si:H with neutral strain and 0.5% compressive and tensile strains, and measurements of a-Si:H on c-Si with neutral strain and 0.33% compressive strain, with peaks blueshifted by compressive strain and *vice versa*.

(LO) shoulder near 400 cm^{-1} is also in good agreement. The low-energy spectrum agrees less well due to the more delocalized modes [25] and sensitivity to the size of the calculated supercells. The strong peak at 520 cm^{-1} in the experiment is due to the underlying c-Si substrate, which also has a small peak at 300 cm^{-1} due to second-order Raman scattering [47]. After a linear baseline correction, the experimental Raman spectra were fit to a sum of 3 Gaussians for the a-Si:H features [30] and a Lorentzian for c-Si [47] according to standard practice; LO and TO fits are shown in Fig. 1 and the Supplemental Material [34]. We underscore the significant improvement in theoretical agreement with experiment compared to the previous DFT/semiempirical Raman work [29] which underestimated the TO peak by 50 cm^{-1} and did not show the other peaks. We can now quantitatively predict the strain effects on the spectrum.

We now focus on the region 400–550 cm^{-1} around the a-Si:H TO peak and c-Si optical modes and add the calculated spectra under 0.5% compressive and tensile uniaxial strains, and the measured spectrum under 0.33% compressive uniaxial strain, as shown in Fig. 2. The shifts to lower energies under tensile strain and higher energies under compressive strain can be seen in theory and experiment, for both the a-Si:H and c-Si peaks.

To analyze the strain effect in a-Si:H in our calculation, we make a one-to-one correspondence between the discrete vibrational modes in a supercell structure at each strain level. We find the Raman intensity change with strain is a small and almost uniform scaling over the spectrum. As a result, the strain effect on peak positions can be described by considering just the vibrational frequencies. The $\pm 0.5\%$ strain was confirmed to be in the linear regime by plotting frequencies over a range of strains.

For each mode in each structure, we compute the derivatives of the frequency in the compressive and tensile strain directions. These derivatives are closely related to the mode Grüneisen parameters $\gamma = -\frac{1}{\omega}\frac{d\omega}{d\epsilon}$ and are shown in full in the Supplemental Material [34]. We perform an average (weighted by the Raman intensities) over the derivatives of modes with frequencies 450–490 cm^{-1}, yielding an overall TO

peak position derivative of 460 ± 10 cm^{-1}. The uncertainty is taken as the standard error of the mean, taking only the different structures as independent.

It is difficult to determine the strain sufficiently accurately from our wafer curvature via Stoney's equation [48], and this would give only an averaged strain over the wafer. Instead we use the c-Si Raman shifts as an internal calibration of the local strain at the beam spot. We exploit the fact that our Raman measurements show both the a-Si:H thin film and the top of the underlying c-Si substrate (Fig. 1), given the penetration depth of 1 μm at 632.8 nm for a-Si:H and c-Si [2].

To perform the calibration, we relate the c-Si peak shift to uniaxial strain according to the approach of Refs. [49] and [20]. The geometry of our four-point bending setup (inset in Fig. 1), results in uniaxial stress in [110] (x) in the roughly rectangular region between the rods, according to the usual plane stress assumptions [50]. The optical mode detected in our backscattering geometry is shifted from the unstrained frequency $\omega_0^c = 520$ cm^{-1} [43] proportionally to the strain ϵ_{xx} as $\Delta\omega^c = b\epsilon_{xx}$, where

$$b = \left[-p\nu_{xz}^c + q\left(1 - \nu_{xy}^c\right)\right]/2\omega_0^c = -330 \pm 70 \text{ cm}^{-1} \quad (1)$$

(derived in the Supplemental Material [34]). We use c-Si Poisson ratios $\nu_{xy}^c = 0.064$ and $\nu_{xz}^c = 0.28$ [51] and the strain coefficients $p = -1.25 \pm 0.25\,(\omega_0^c)^2$ and $q = -1.87 \pm 0.37(\omega_0^c)^2$ from an experiment with the same 632.8 nm excitation as in this work [23]. Due to stress relaxation (i.e., greater ν_{xz}^c) near the surface, these strain coefficients are lower than those obtained at 1064 nm [24], with a signal penetrating about 100 μm into the bulk [2].

Next we connect the strain in c-Si to the strain in the a-Si:H film, specifically the trace $\text{Tr}\,\epsilon^a$ (justified below). Assuming no slip from the substrate, the strain ϵ_{xx} is the same in the a-Si:H film. Taking into account the other directions,

$$\text{Tr}\,\epsilon^a = d\epsilon_{xx} = \left(1 - \nu_{xy}^c - \nu^a\right)\epsilon_{xx}, \quad (2)$$

where the coefficient $d = 0.69 \pm 0.05$, using $\nu^a = 0.25 \pm 0.05$ for dense films of 10% H [52].

We now infer strain for each position of the four-point bending setup from the c-Si peak shift as $\text{Tr}\,\epsilon^a = d\Delta\omega^c/b$. Given a Young's modulus around 80 GPa [53] and strain 0.33%, maximum stress was 260 MPa, well within the range from PECVD growth [14]. We plot the experimental a-Si:H peak position with respect to strain in Fig. 3, showing a linear relationship with regression slope -510 ± 120 cm^{-1}; the uncertainty is mostly from the c-Si calibration values and ν^a. The plotted line with the theoretical slope (and experimental intercept) also fits the data well. Note that if uniaxial strain rather than stress had been assumed in the wafer, we would have obtained $b = q/2\omega_0^c$ and $d = 1$, yielding almost the same value $s = -520 \pm 110$ cm^{-1}, showing insensitivity to the exact mechanical boundary conditions. We quote our result with respect to strain, rather than stress, to be more general since the shifts are due directly to bond length changes, and the Young's modulus relating stress and strain can vary by a factor of 2 depending on synthesis conditions [53].

Finally, we demonstrate the general form of the a-Si:H TO peak shift with strain. c-Si has a complicated dependence on the strain pattern due to its symmetry, but a-Si:H is isotropic
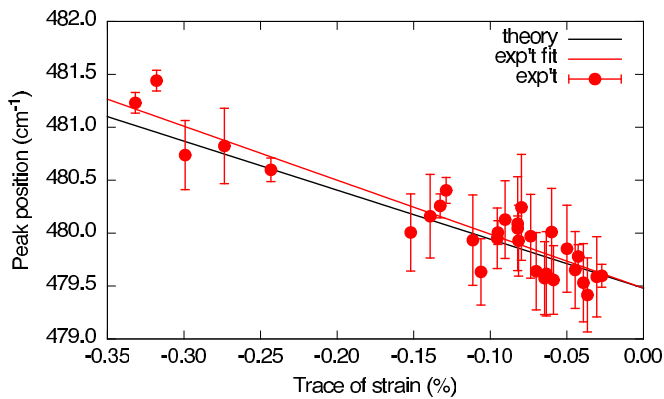
FIG. 3. (Color online) Shifts in *a*-Si:H Raman peak positions vs strain from uniaxial stress, inferred from *c*-Si peak shifts. Slopes: -460 ± 10 cm^{-1} (theory), -510 ± 120 cm^{-1} (exp't fit). Both lines use experimental intercept. Relation can be used to infer local strain from Raman microscopy.

except at very short length scales. For example, in our 70-atom cells, the calculated dielectric constant is ~ 15 with anisotropy only ~ 0.6. Due to this effective symmetry, the calculated vibrational modes in the TO peak are delocalized, roughly isotropic, and sensitive to Raman scattering in any polarization (see inset of Fig. 1). Nonetheless, without any true symmetry, there is no counterpart to the threefold degeneracy of the *c*-Si optical phonons. As a result, the TO band transforms as a scalar rather than a vector as for *c*-Si. Since there is no degeneracy, there is no splitting as of the *c*-Si modes [23]. In general, the frequency shift for such a scalar mode in a material would be $\Delta\omega = \sum_{ij} S_{ij}\epsilon_{ij}$ where S, like ϵ, is a symmetric rank-2 tensor. For an isotropic material, symmetry dictates $S_{ij} = s\delta_{ij}$. Therefore the peak shift is determined only by the trace of the strain tensor:

$$\Delta\omega^a = s\left(\epsilon_{xx}^a + \epsilon_{yy}^a + \epsilon_{zz}^a\right) = s \, \mathrm{Tr} \, \epsilon^a. \qquad (3)$$

Indeed, we find in our calculations that the Raman spectrum is almost indistinguishable for applied uniaxial, biaxial, or triaxial strain tensors with the same trace, even on a single 70-atom cell [34]. This analysis applies generally to isotropic amorphous vibrational modes.

We find that our theoretical (-460 ± 10 cm^{-1}) and experimental (-510 ± 120 cm^{-1}) values are consistent, supporting the accuracy of the results. The agreement also implies lack of slip between the *a*-Si:H film and *c*-Si substrate, as has been argued for thermal expansion of epitaxial graphene [54], as slip would relax strain and lower the measured coefficient. The value is similar to the isotropic one for *c*-Si (surface), -430 ± 90 cm^{-1} [23].

TABLE I. Raman transverse optical (TO) peak positions ω and mode Grüneisen parameters γ for crystalline (*c*) and amorphous (*a*) Si from: DFT, DFT plus bond polarizability model, experiment, and classical potentials. From this work unless cited.

	DFT	Model	Exp't	Classical [25]
ω_c/cm^{-1}	514		520 [43]	605
ω_a/cm^{-1}	470	430 [29]	480	525
γ_c	0.98		1.08 [24]	0.8
γ_a	0.98		1.06	1.0

In Table I we compare theoretical and experiment results for peak frequencies and mode Grüneisen parameters γ of *c*-Si and *a*-Si:H. γ, describing anharmonicity, is important in the theory of thermal expansion and phonon transport [25,55]. The importance of *ab initio* calculations is shown by the much improved agreement with experimental ω and γ, compared to classical potentials [25].

To conclude, we obtained the Raman spectra of *a*-Si:H from first principles in good agreement with experiment. We computed the strain coefficient for the TO peak from theory as -460 ± 10 cm^{-1}, and measured a consistent value of -510 ± 120 cm^{-1}, achieving an experimental uncertainty similar to that for *c*-Si surfaces despite having to deconvolve much broader peaks. We demonstrated, by symmetry analysis and explicit computation, the general form of strain effects on isotropic amorphous vibrational mode frequencies, as $\Delta\omega = s \, \mathrm{Tr} \, \epsilon$, determined only by the trace of the strain. The actual strain pattern (as in *c*-Si) needs to be provided by elasticity modeling [20]. Our results provide consistent and reliable calibration for the Raman/strain relation, enabling micro-Raman mapping of strain in *a*-Si:H films for the further development of photovoltaic, electronic, and mechanical devices.

[1] J. Jean, P. R. Brown, R. L. Jaffe, T. Buonassisi, and V. Bulović, Pathways for solar photovoltaics, Energy Environ. Sci. **8**, 1200 (2015).

[2] A. Shah, Thin-film silicon solar cells, in *Solar Cells*, edited by T. Markvart, A. McEvoy, and L. Castañer, 2nd ed. (Elsevier, Boston, 2013), Chap. IC-1, pp. 159–223.

[3] B. M. George, J. Behrends, A. Schnegg, T. F. Schulze, M. Fehr, L. Korte, B. Rech, K. Lips, M. Rohrmüller, E. Rauls *et al.*, Atomic Structure of Interface States in Silicon Heterojunction Solar Cells, Phys. Rev. Lett. **110**, 136803 (2013).

[4] F. F. Abdi, L. Han, A. H. M. Smets, M. Zeman, B. Dam, and R. Van de Krol, Efficient solar water splitting by enhanced charge

separation in a bismuth vanadate-silicon tandem photoelectrode, Nat. Commun. **4**, 2195 (2013).

[5] H. Gleskova and S. Wagner, Electron mobility in amorphous silicon thin-film transistors under compressive strain, Appl. Phys. Lett. **79**, 3347 (2001).

[6] A. J. Syllaios, T. R. Schimert, R. W. Gooch, W. L. McCardel, B. A. Ritchey, and J. H. Tregilgas, Amorphous silicon microbolometer technology, MRS Proc. **609**, A14.4 (2000).

[7] A. Franco, Y. Riesen, M. Despeisse, N. Wyrsch, and C. Ballif, High spatial resolution of thin-film-on-ASIC particle detectors, IEEE Trans. Nucl. Sci. **59**, 2614 (2012).

[8] S. Chang and S. Sivoththaman, Development of a low temperature MEMS process with a PECVD amorphous silicon structural layer, J. Micromech. Microeng. **16**, 1307 (2006).

[9] D. L. Staebler and C. R. Wronski, Reversible conductivity changes in discharge-produced amorphous Si, Appl. Phys. Lett. **31**, 292 (1977).

[10] J. Mattheis, J. H. Werner, and U. Rau, Finite mobility effects on the radiative efficiency limit of *pn*-junction solar cells, Phys. Rev. B **77**, 085203 (2008).

[11] A. H. Mahan, M. S. Dabney, D. Molina Piper, and W. Nemeth, The effect of film tensile stress on crystallite nucleation and growth in thermally annealed a-Si:H, J. Appl. Phys. **115**, 083502 (2014).

[12] K. Wu, X. Q. Yan, and M. W. Chen, *In situ* Raman characterization of reversible phase transition in stress-induced amorphous silicon, Appl. Phys. Lett. **91**, 101903 (2007).

[13] N. Tabet, A. Al-Sayoud, S. Said, X. Yang, Y. Yang, A. Syed, E. Diallo, Z. Wang, X. Wang, E. Johlin *et al.*, Raman study of localized recrystallization of amorphous silicon induced by laser beam, in *38th IEEE Photovoltaic Specialists Conference* (IEEE, Austin, TX, 2012), pp. 364–366.

[14] E. Johlin, N. Tabet, S. Castro-Galnares, A. Abdallah, M. I. Bertoni, T. Asafa, J. C. Grossman, S. Said, and T. Buonassisi, Structural origins of intrinsic stress in amorphous silicon thin films, Phys. Rev. B **85**, 075202 (2012).

[15] V. Paillard, P. Puech, R. Sirvin, S. Hamma, and P. Roca i Cabarrocas, Measurement of the in-depth stress profile in hydrogenated microcrystalline silicon thin films using Raman spectrometry, J. Appl. Phys. **90**, 3276 (2001).

[16] E. Johlin, C. B. Simmons, T. Buonassisi, and J. C. Grossman, Hole-mobility-limiting atomic structures in hydrogenated amorphous silicon, Phys. Rev. B **90**, 104103 (2014).

[17] M. Stutzmann, Role of mechanical stress in the light-induced degradation of hydrogenated amorphous silicon, Appl. Phys. Lett. **47**, 21 (1985).

[18] J. Pomeroy, P. Gkotsis, M. Zhu, G. Leighton, P. Kirby, and M. Kuball, Dynamic operational stress measurement of MEMS using time-resolved Raman spectroscopy, J. Microelectromech. Syst. **17**, 1315 (2008).

[19] J. Feng, X. Qian, C.-W. Huang, and J. Li, Strain-engineered artificial atom as a broad-spectrum solar energy funnel, Nat. Photon. **6**, 866 (2012).

[20] I. De Wolf, Micro-Raman spectroscopy to study local mechanical stress in silicon integrated circuits, Semicond. Sci. Technol. **11**, 139 (1996).

[21] E. Bonera, M. Fanciulli, and D. N. Batchelder, Combining high resolution and tensorial analysis in Raman stress measurements of silicon, J. Appl. Phys. **94**, 2729 (2003).

[22] X. L. Wu, S. Tong, X. N. Liu, X. M. Bao, S. S. Jiang, D. Feng, and G. G. Siu, X-ray diffraction study of alternating nanocrystalline silicon/amorphous silicon multilayers, Appl. Phys. Lett. **70**, 838 (1997).

[23] E. Anastassakis, A. Pinczuk, E. Burstein, F. Pollak, and M. Cardona, Effect of static uniaxial stress on the Raman spectrum of silicon, Solid State Commun. **8**, 133 (1970).

[24] E. Anastassakis, A. Cantarero, and M. Cardona, Piezo-Raman measurements and anharmonic parameters in silicon and diamond, Phys. Rev. B **41**, 7529 (1990).

[25] J. Fabian and P. B. Allen, Thermal Expansion and Grüneisen Parameters of Amorphous Silicon: A Realistic Model Calculation, Phys. Rev. Lett. **79**, 1885 (1997).

[26] E. Anastassakis, Strain characterization of semiconductor structures and superlattices, in *Light Scattering in Semiconductor Structures and Superlattices*, edited by D. J. Lockwood and J. F. Young (Springer, New York, 1991), Vol. 273 of *NATO ASI Series*, pp. 173–196.

[27] J.-K. Shin, C. S. Lee, K.-R. Lee, and K. Y. Eun, Effect of residual stress on the Raman-spectrum analysis of tetrahedral amorphous carbon films, Appl. Phys. Lett. **78**, 631 (2001).

[28] G. Gouadec and P. Colomban, Raman spectroscopy of nanomaterials: How spectra relate to disorder, particle size and mechanical properties, Prog. Cryst. Growth Charact. Mater. **53**, 1 (2007).

[29] R. M. Ribeiro, V. J. B. Torres, M. I. Vasilevskiy, A. Barros, and P. R. Briddon, Ab-initio modeling of a-Si and a-Si:H, Phys. Stat. Sol. (c) **7**, 1432 (2010).

[30] T. Ishidate, K. Inoue, K. Tsuji, and S. Minomura, Raman scattering in hydrogenated amorphous silicon under high pressure, Solid State Commun. **42**, 197 (1982).

[31] Y. Hishikawa, Raman study on the variation of the silicon network of a-Si:H, J. Appl. Phys. **62**, 3150 (1987).

[32] Y. Hishikawa (private communication).

[33] A. Vetushka, M. Ledinský, J. Stuchlík, T. Mates, A. Fejfar, and J. Kočka, Mapping of mechanical stress in silicon thin films on silicon cantilevers by Raman microspectroscopy, J. Non-Cryst. Solids **354**, 2235 (2008).

[34] See Supplemental Material at http://link.aps.org/supplemental/10.1103/PhysRevB.92.241202 for more details on theoretical calculations, atomic coordinates, experimental methods, strain modeling, and strain mapping.

[35] F. Wooten, K. Winer, and D. Weaire, Computer Generation of Structural Models of Amorphous Si and Ge, Phys. Rev. Lett. **54**, 1392 (1985).

[36] E. Johlin, L. K. Wagner, T. Buonassisi, and J. C. Grossman, Origins of Structural Hole Traps in Hydrogenated Amorphous Silicon, Phys. Rev. Lett. **110**, 146805 (2013).

[37] L. K. Wagner and J. C. Grossman, Microscopic Description of Light Induced Defects in Amorphous Silicon Solar Cells, Phys. Rev. Lett. **101**, 265501 (2008).

[38] D. A. Strubbe, L. K. Wagner, E. C. Johlin, and J. C. Grossman, Computational hydrogenated amorphous semiconductor structure maker (CHASSM) (unpublished).

[39] S. Baroni, S. de Gironcoli, A. Dal Corso, and P. Giannozzi, Phonons and related crystal properties from density-functional perturbation theory, Rev. Mod. Phys. **73**, 515 (2001).

[40] P. Giannozzi, S. Baroni, N. Bonini, M. Calandra, R. Car, C. Cavazzoni, D. Ceresoli, G. L. Chiarotti, M. Cococcioni, I. Dabo *et al.*, QUANTUM ESPRESSO: a modular and

open-source software project for quantum simulations of materials, J. Phys.: Condens. Matter **21**, 395502 (2009).

[41] J. P. Perdew and A. Zunger, Self-interaction correction to density-functional approximations for many-electron systems, Phys. Rev. B **23**, 5048 (1981).

[42] M. Lazzeri and F. Mauri, First-Principles Calculation of Vibrational Raman Spectra in Large Systems: Signature of Small Rings in Crystalline SiO_2, Phys. Rev. Lett. **90**, 036401 (2003).

[43] J. H. Parker, D. W. Feldman, and M. Ashkin, Raman scattering by silicon and germanium, Phys. Rev. **155**, 712 (1967).

[44] X. J. Gu, Simultaneous measurements of Stokes and anti-Stokes Raman spectra for thermal characterization of diode laser facet, J. Raman Spectrosc. **27**, 83 (1996).

[45] J. E. Smith, M. H. Brodsky, B. L. Crowder, M. I. Nathan, and A. Pinczuk, Raman Spectra of Amorphous Si and Related Tetrahedrally Bonded Semiconductors, Phys. Rev. Lett. **26**, 642 (1971).

[46] M. H. Brodsky, M. Cardona, and J. J. Cuomo, Infrared and Raman spectra of the silicon-hydrogen bonds in amorphous silicon prepared by glow discharge and sputtering, Phys. Rev. B **16**, 3556 (1977).

[47] P. A. Temple and C. E. Hathaway, Multiphonon Raman spectrum of silicon, Phys. Rev. B **7**, 3685 (1973).

[48] L. B. Freund and S. Suresh, *Thin Film Materials* (Cambridge University Press, New York, 2003).

[49] S. Ganesan, A. Maradudin, and J. Oitmaa, A lattice theory of morphic effects in crystals of the diamond structure, Ann. Phys. **56**, 556 (1970).

[50] L. L. Bucciarelli Jr., *Engineering Mechanics of Solids: A First Course in Engineering* (2002), http://web.mit.edu/emech/dontindex-build/full-text/emechbk_7.pdf.

[51] M. Hopcroft, W. Nix, and T. Kenny, What is the Young's modulus of silicon? J. Microelectromech. Syst. **19**, 229 (2010).

[52] R. Kuschnereit, H. Fath, A. Kolomenskii, M. Szabadi, and P. Hess, Mechanical and elastic properties of amorphous hydrogenated silicon films studied by broadband surface acoustic wave spectroscopy, Appl. Phys. A **61**, 269 (1995).

[53] X. Jiang, B. Goranchev, K. Schmidt, P. Grünberg, and K. Reichelt, Mechanical properties of a-Si:H films studied by Brillouin scattering and nanoindenter, J. Appl. Phys. **67**, 6772 (1990).

[54] N. Ferralis, R. Maboudian, and C. Carraro, Determination of substrate pinning in epitaxial and supported graphene layers via Raman scattering, Phys. Rev. B **83**, 081410 (2011).

[55] K. Esfarjani, G. Chen, and H. T. Stokes, Heat transport in silicon from first-principles calculations, Phys. Rev. B **84**, 085204 (2011).